University of Cambridge
Department of Engineering
Trumpington Street
Cambridge, CB2 1PZ, UK

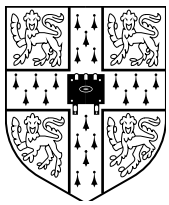

Ashby Chart inspired design of tall modular buildings

CUED/D-STRUCT/TR.251

July 2018

P S Tzokova · K A Seffen · J M Lees

ISSN: 0309-7447

Abstract

Ashby Charts have been used extensively in the past, mainly for the design of materials and structural sections. The main aim of this paper is to extend the Ashby Chart design methodology to an overall structural level. As an example, this methodology is applied to modular buildings, considering several different steel module topologies; thin-walled boxes, unbraced frames and braced frames, stacked to create modular towers. The ultimate limit state (strength and buckling) and serviceability limit state (horizontal deflection) are considered to find the height of tower at failure. The results are plotted as an Ashby-inspired Chart, showing maximum tower height vs module weight. It is intended that this chart be used as an initial design tool when designing tall modular buildings, and similar charts can be derived for other types of structure as well. It is found that the best performing realistic steel module topology is the unbraced frame, which would be chosen as an initial design. This result is investigated further using a robustness analysis, again with an Ashby approach.

1 Introduction

Ashby Charts have been used extensively in the past for many purposes. The charts were first devised by Ashby (1989, 2005) and developed by Ashby et al. (Ashby and Brechet 2003; Wegst and Ashby 2004; Ashby and Greer 2006) for structural material design. They were later expanded by Weaver and Ashby (1996, 1998) to structural section design.

These charts are used to map the efficiency of materials and structural sections for a particular pair of metrics, often plotting boundaries around clusters of data of a certain type, *e.g.* structural sections made from different materials. Ashby had previously devised similar charts such as deformation mechanism charts (Ashby 1972; Crossman and Ashby 1975), fracture mechanism charts (Ashby, Gandhi and Taplin 1979; Gandhi and Ashby 1979) and wear mechanism charts (Lim and Ashby 1987), but the main Ashby Chart methodology did not arise until the material design charts.

Others have also developed Ashby's material and structural section charts further (Holloway 1998; Counts et al. 2009, 2010; Begley et al. 2012; Sobczak, Lang and Haider 2012; Shah 2013; Birmingham and Wilcox 1993; Birmingham et al. 1994) as well as the deformation, fracture and wear mechanism charts (Liu, Asthana and Rohatgi 1991; Malakondaiah and Rama Rao 1981, 1982). New forms of Ashby Charts have also been developed, such as 'Dynamic Ashby Charts' (Nemat-Nasser et al. 2011) and 'Ashby Refrigerant Maps' (Sandeman 2012).

In this study, we also develop our own Ashby-inspired Charts for structural design beyond material and section levels: Fig. 1 shows a rudimentary view of our position within the structural hierarchy.

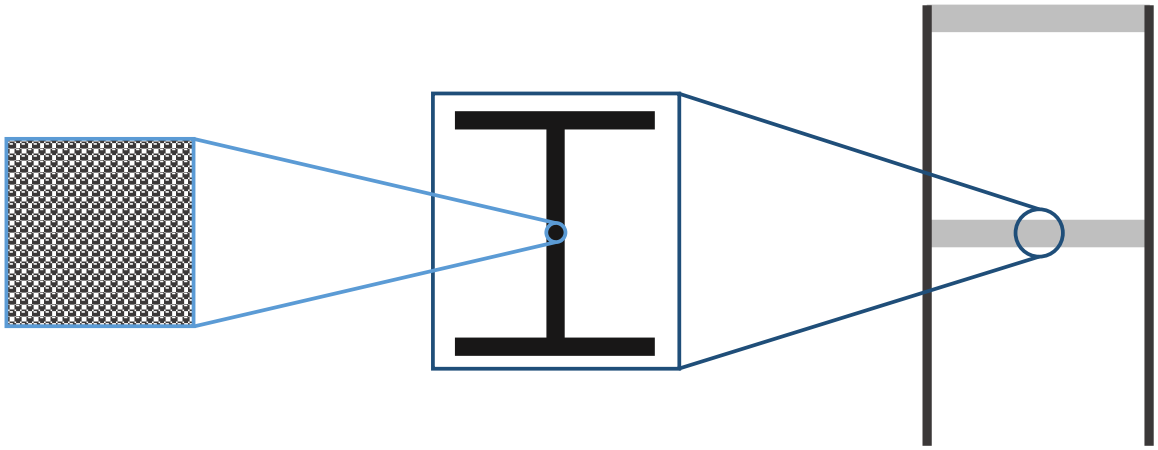

FIGURE 1: Ashby Chart hierarchy. Original material level (left), developed by Ashby to a structural section level (middle) and finally here expanded further to an overall structure level (right)

The structural form of modular buildings is used as an example, since the discrete modules can be treated as components of the building, which is useful when considering an Ashby design approach. Our metric is the tallest height possible of modular tower. An example of a tall modular building is shown in Fig. 2.

FIGURE 2: An example of a high-rise modular building with 24 storeys: Victoria Hall student residence in Wolverhampton, UK (Edkins 2014)

1.1 Ashby philosophy

The Ashby design approach for designing a structural component involves firstly considering the function of the component being designed, *e.g.* performing as a beam in bending or as a column carrying an axial force. Next, the designer has an objective – making the component as light or as cheap as possible, for example. This is done by deriving an objective function and finding an index to be maximised. This objective is a mathematical function, usually in the form of a power law exponential from dimensionless analysis or some other analysis where the scale of the problem is conveniently expressed. In Weaver and Ashby (1996), for example, the authors normalise the behaviour of the structural section with respect to a solid circular section – a reference shape, where most other sections have a 'shape factor' above unity. The design process will invariably have constraints, continuous or discrete in value, such as plate thicknesses, material properties, etc. We describe our philosophy momentarily.

1.2 Material, module and building

Modules are generally room-sized, on average 3.5 m × 10 m × 2.8 m high. Currently, the favoured material for these is structural steel but timber and concrete modules are also used (Gorgolewski, Grubb and Lawson 2001). Lighter materials are advantageous for lifting modules into place more easily.

Three practical and familiar steel module topologies, shown in Fig. 3, are selected for investigation. In addition, a 'solid' block module is used for reference, Fig. 3(a). The walls of real thin-walled box modules, Fig. 3(b), are typically made from C-section studs (Gorgolewski, Grubb and Lawson 2001), whereas the braced and unbraced frame modules, Figs 3(c) & (d), usually have columns made from square hollow sections (Lawson 2007). For analysis purposes, these modules are idealised as shown in Fig. 3.

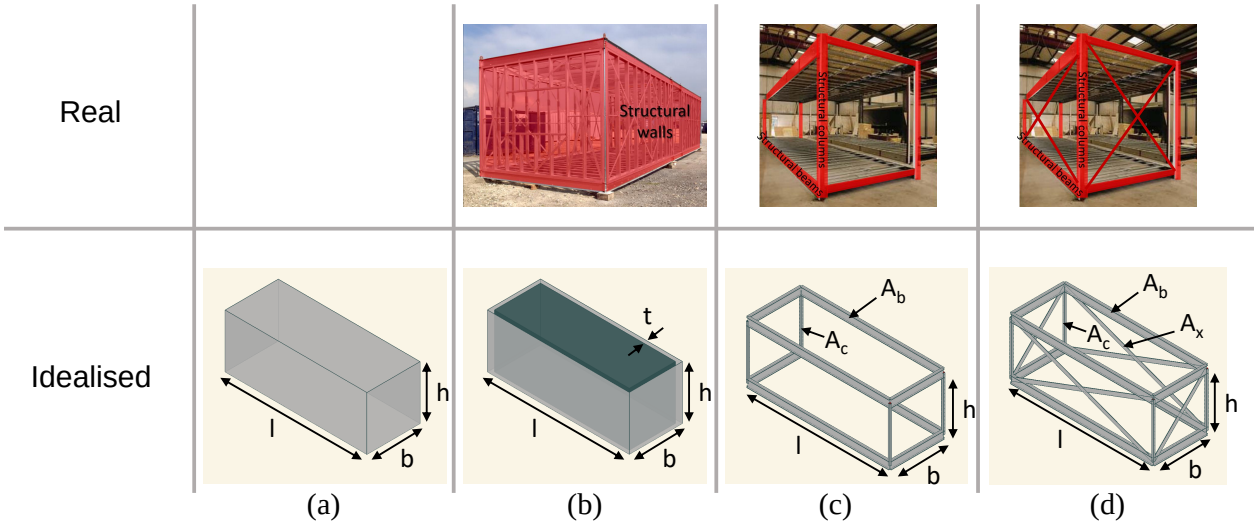

FIGURE 3: Modules used in practice (real) (Kingspan Steel Building Solutions 2007, 2012) and modules in this analysis (idealised, modelled in Oasys GSA (Arup 2015)): **(a)** solid block module, note this is only used for comparison with other module topologies in this analysis and hence has no real equivalent; **(b)** thin-walled box module, the walls of which behave as structural plates; **(c)** unbraced frame module with fully fixed moment connections; **(d)** braced frame module with pinned connections

Modular construction involves stacking modules on top of each other, or placing non-structural modules on a separate structural frame, or a combination of these where stacks of several modules are placed on a frame. Typically, the modules support themselves under gravity loads, while a separate frame or core resists lateral loads (Lawson 2007). In the proposed analysis, a modular tower with a single module footprint, which supports itself under both gravity and lateral loads, is considered because it is a simple system for demonstrating our methodology. If this basic building type can be understood, it may be combined with an external frame or core, for extra strength and stability in real modular buildings.

Each module performs several structural functions, including carrying bending moments, axial forces and compressive and tensile stresses; our objective is to maximise the number of storeys. The major constraints are that the module must not exceed limits due to material failure or buckling and that the resulting modular tower must not exceed a certain deflection limit.

A large number of design variable combinations are considered, such as module and section size. The loads in the sections at the base of the structure are compared to their capacity, and overall lateral deflection limits are considered; other practical limitations and constraints are beyond the scope of study.

2 Methods and calculation

Strength, stability and deflection limits are chosen to demonstrate our structural Ashby-inspired Charts, which will provide an initial concept design. Other limits can later be incorporated, as the design becomes more detailed.

2.1 Ashby design approach limitations

We attempt to extend the Ashby design approach for structural components to an overall structure: we want to find the best structure, given a desired performance. We start by considering a single module from a modular building. Modules are 2D structural frames, either braced or unbraced, as shown in Fig. 4. These have just a few structural sections, so seem a natural step up from the individual structural sections considered by Weaver and Ashby (1996).

The objective function we seek to minimise is the deflection due to a lateral point load, as shown in Fig. 4, representing a nominal wind load. Here, we demonstrate the limitations of the Ashby approach for frames, via a trivial example. We consider a simple square frame, with all members having cross-sectional area A and length L, as shown in Fig. 4. Minimising deflections is tantamount to maximising the stiffness, which can be derived as follows:

$$S_{braced} = \frac{F}{\delta_{braced}} = \frac{EA}{(2+2\sqrt{2})L}, \quad S_{unbraced} = \frac{F}{\delta_{unbraced}} = \frac{4EI}{L^3} \tag{1}$$

Ashby's shape factor for elastic bending ($\phi_b = 4\pi I/A^2$) can be incorporated into the stiffness for the unbraced frame. We develop a different dimensionless ϕ defined as $\phi_o = A/L^2$. Since the cross-sectional area is independent of the length completely, ϕ_o is not normalised with respect to any one section. Both ϕ expressions are substituted in, eliminating I and A:

$$S_{braced} = \frac{EL\phi_o}{2+2\sqrt{2}}, \quad S_{unbraced} = \frac{EL\phi_b\phi_o^2}{\pi} \tag{2}$$

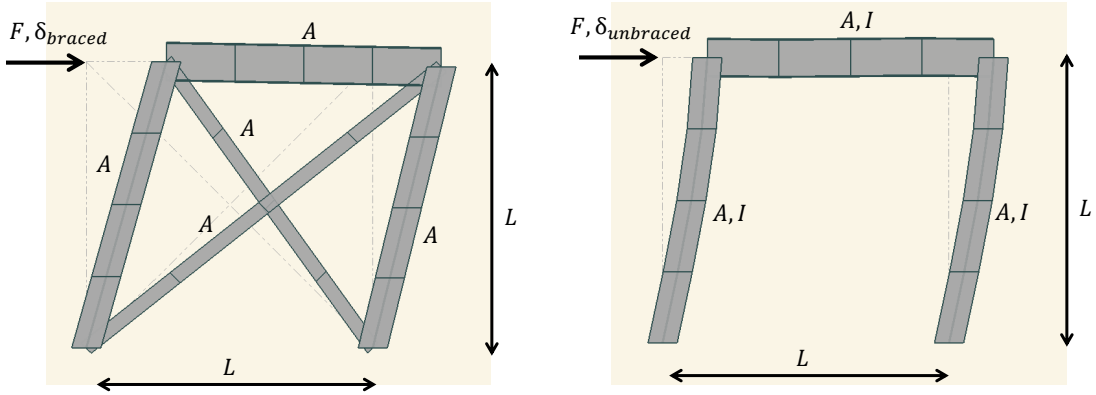

(a) (b)

FIGURE 4: Structural frames. **(a)** Braced frame, with pinned joints. Deflection is calculated by considering the frame as a truss. Note that the compression bracing member is assumed inactive. **(b)** Unbraced frame, with fixed beam to column connections and pinned feet. Deflection is calculated by considering the frame bending under the loading. All members have cross-sectional area A and second moment of area I (although I is not relevant in the braced case). Height and width of the frame are L

The braced frame can be considered as a reference structure, much like Ashby's solid circular reference cross-section. This results in the following structural index that we call ϕ_f, from which braced and unbraced frames can be compared:

$$\phi_f = \frac{S_{unbraced}}{S_{braced}} = \frac{(2+2\sqrt{2})}{\pi}\phi_b\phi_o \tag{3}$$

If this value is above unity, then an unbraced frame outperforms a braced frame for maximum stiffness (minimum deflection) and vice versa. For example, take a 2 m × 2 m frame where all the sections are UC 203 × 203 × 52:

$$\begin{aligned} \phi_b &= 4\pi I/A^2 = 15.0 \\ \phi_o &= A/L^2 = 1.66 \times 10^{-3} \\ \phi_f &= \frac{(2+2\sqrt{2})}{\pi}\phi_b\phi_o = 0.0383 \end{aligned} \tag{4}$$

Therefore, the braced frame greatly outperforms the unbraced as we might expect for a single frame.

The structural index, ϕ_f, is similar in concept to a different structural index proposed by Shanley (1960): both indices attempt to normalise some structural aspect. Shanley's structural index has units of stress and is a measure of the loading intensity, while also eliminating size effects. It therefore varies from ϕ_f which is dimensionless and compares the stiffness of an unbraced frame to a braced frame. Here, we are trying to maximise stiffness, which is a structural property and independent of loading magnitude. We could use Shanley's structural index if, for example, we were trying to minimise mass or cost.

The Ashby approach would then proceed to plot the structural index, ϕ_f, of many different frames on a chart. The original Ashby Charts for structural sections plotted values of ϕ_b on axes of I and A, the two section properties it depends on. Here, ϕ_f, in terms of ϕ_o and ϕ_b, depends on the values of I, A *and* L. Three axes are required, resulting in a three dimensional chart. Constant values of ϕ_f on log-log axes would be represented as inclined planes of the form $I = A + 2L + \text{constant}$.

However, recall that all members in the frames used to find ϕ_f above are the same. It is desirable to extend this approach to frames where the different components of the frames have different cross-sectional areas and lengths. The calculation to find the equivalent ϕ_f is more involved, and does not result in a simple expression as the ϕ_f above. Namely, we now have two variables for each of L, A and I, hence six variables overall. We would therefore need six axes, and so a meaningful design chart is no longer possible.

Also, the overall objective is to maximise the number of storeys of each tower, and we have so far only considered a single storey. The deflections of braced and unbraced frames behave differently as more storeys are stacked, further complicating the analysis above by adding another variable – number of storeys. Furthermore, we are interested in analysing the frames for strength and buckling as well as stiffness, for which objective functions and comparisons like those above would be possible, but each member would have to still be checked for failure separately.

The analysis required to achieve similar ϕ_f expressions to that above with all the constraints mentioned is envisaged to be more complicated than following a traditional design route. Therefore, the analysis was continued in a traditional manner, by finding the maximum number of storeys achievable by each module, which is within the constraints of material failure, buckling and deflection. However, the charts plotted are still 'Ashby-inspired' because of their presentation – on log-log axes with clusters of different structural module topologies (see Section 3). The essence of the Ashby design approach is also present since we use a reference solid block module – its performance is compared to the performance of other modules, but in a less official way than using the shape and scale factors above to derive indices.

2.2 Traditional design approach

The structural behaviour of a vertically stacked tower of single modules is considered for strength (material failure), stability and stiffness, in order to find the maximum tower height at failure. Two analyses are performed: the calculation of the ultimate limit state (ULS) taking into account material failure and buckling (stability); and the serviceability limit state (SLS) as defined by a maximum lateral deflection of the top of the building equal to 1/500 times the building height (ASCE 1988). Unless otherwise stated, perfect connections between modules are assumed. Both vertical and horizontal loads are considered in isolation, and also in combination, and the worst case is chosen. Unfactored loads and resistances are used throughout. The vertical gravity loads are the self-weight of the structure plus an imposed floor load of $1.5\,\text{kN/m}^2$, from

Eurocode 1 (BSI 2005). The imposed lateral load is assumed to be a wind load of $1\,\mathrm{kN/m^2}$, equivalent to a conservative wind speed of $40\,\mathrm{m/s}$, and is applied as equal point loads at each storey, as demonstrated in Fig. 5, which also shows the resulting base shear and moment. The wind load is applied in turn to two perpendicular vertical faces of the tower, after which the critical wind load direction can be found for each failure mode.

FIGURE 5: Example modular tower displaying the discrete wind loads at each storey and the resulting base shear and moment

2.3 Assumptions

Second order geometrical effects are omitted for simplicity but could be considered and incorporated into the Ashby-inspired Charts if they are significant. Braced frames are assumed to be pinned everywhere and, where relevant, the columns are always considered to bend about their minor axis in order to be conservative. Moment connections are assumed to be infinitely strong and infinitely stiff for simplicity so our results may over-estimate the capacity of the unbraced frames. All modules in a tower are assumed to be identical; this is not a very efficient use of material in taller buildings where lighter modules higher up would be more structurally economical, and is again a simplification for analysis.

2.4 Material failure

Stresses are greatest at the bottommost storey of each tower. The normal stresses at the base are calculated by assuming that the maximum compressive stress generated from gravity loads and the maximum applied bending moment due to the wind loading act concurrently, resulting in the highest normal stresses at the base. Similarly, shear stresses from wind-induced shear forces are also largest at the base. Normal stresses and shear stresses are then considered in combination using simple yield criteria. Figure 6 shows all of the module components at the bottommost storey for each module topology which are checked for material failure; these are discussed in the following sections.

2.4.1 Solid block modules

The overall normal stress at the base of the tower, area (1) in Fig. 6(a), σ, should be less than the steel yield strength, σ_y, to avoid failure due to yielding. For a module of width b (m), length l (m), and weight w (kN), the first stress component of normal stress due to the self-weight of the modules is nw/bl for n storeys. The lateral wind force in the critical wind direction, the direction in which material failure first occurs, acts on the vertical face of the modular tower with largest area, named the transverse direction, hence the wind force per storey in this direction is defined as S_t. For module height h, and second moment of area I for minor axis bending, the second component of stress, due to bending, is $0.5n(n+1)hS_tb/2I$. The final contribution, f, comes from the imposed floor load of $1.5\,\mathrm{kN/m^2}$ and acts on one storey only (the top storey) for the solid blocks. Summing these components results in the following design constraint:

$$\sigma_y \geq \sigma = \frac{nw}{bl} + \frac{0.5n(n+1)hS_tb}{2I} + f \tag{5}$$

For the module dimensions above, and a wind force, S_t, per storey, the shear stress is $\tau = nS_t/bl$, which should be less than the shear yield strength, τ_y, to avoid failure. The largest shear stress again occurs at the base, (1) in Fig. 6(a), and satisfies:

$$\tau_y \geq \tau = \frac{nS_t}{bl} \tag{6}$$

The effects of the normal and shear stresses together on area (1) in Fig. 6(a) are combined using the Tresca yield criterion (Calladine 1985) using principal stresses derived from a Mohr's Circle whose centre is $(\sigma/2, 0)$ and radius is $(\sigma^2/4 + \tau^2)^{\frac{1}{2}}$. The resulting yield inequality is:

$$\left(\sigma_y - \frac{\sigma}{2}\right)^2 \geq \left(\frac{\sigma}{2}\right)^2 + \tau^2 \tag{7}$$

where σ and τ are calculated using Eqns 5 & 6 respectively. The shear stresses are assumed to be small relative to the normal stresses and the combined stresses need to satisfy this constraint to avoid failure.

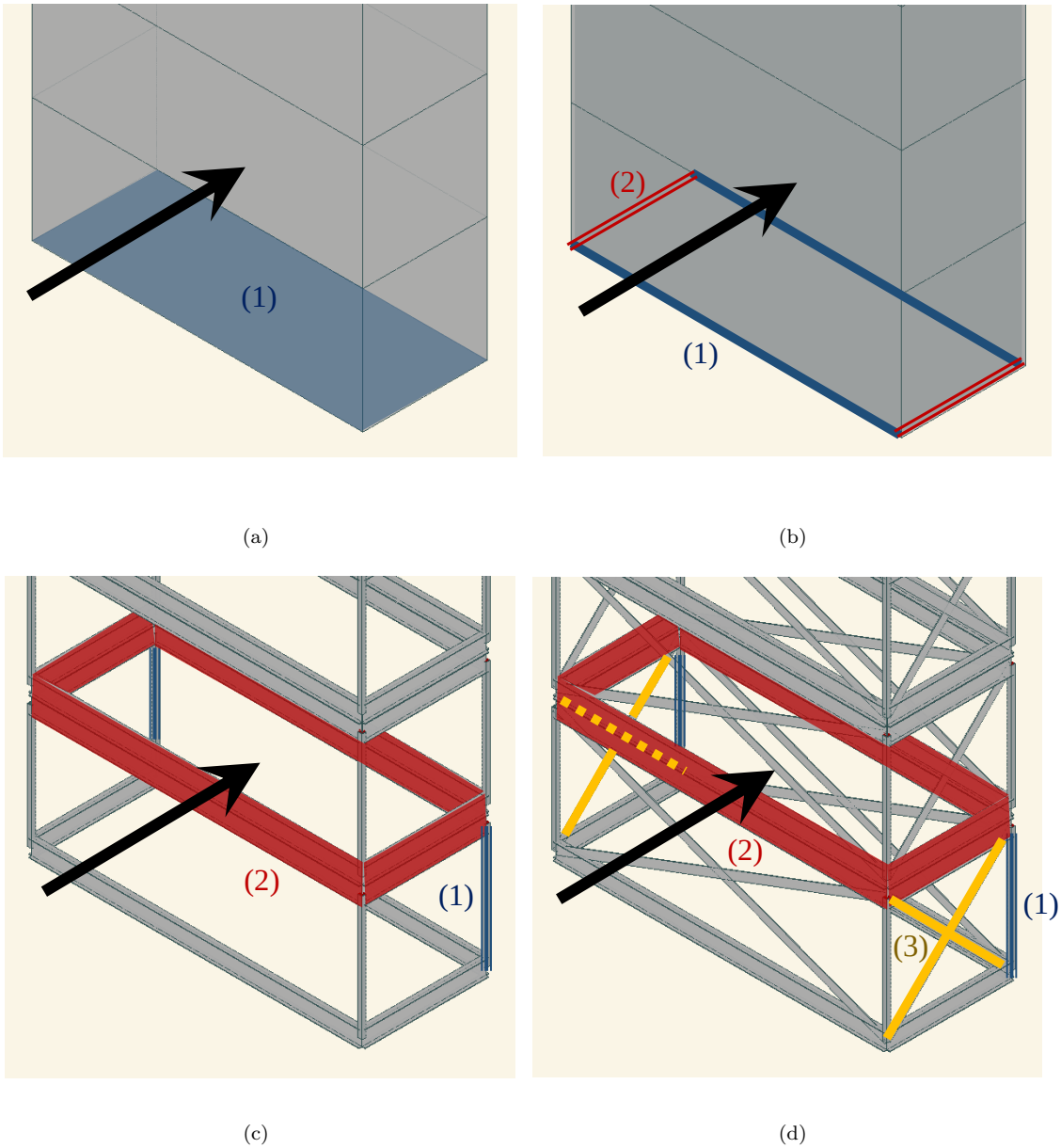

FIGURE 6: Bottommost storeys of modular towers of the four module topologies (Arup 2015), showing the areas and components checked for failure. The black arrows represent the transverse wind direction, which is critical for most cases. **(a)** Solid blocks: (1) base of block; **(b)** thin-walled boxes: (1) flanges, (2) webs; **(c)** unbraced frames: (1) highest loaded columns, (2) "double-height" beams; **(d)** braced frames: (1) highest loaded columns, (2) "double-height" beams, (3) braces (dashed where hidden by other members)

Other module topologies follow a similar calculation of the normal and shear stresses at the base and their subsequent yield criteria.

2.4.2 Thin-walled box modules

For the thin-walled box modules, the normal stresses are calculated assuming that the gravity loads are distributed evenly between each wall. The stresses arising from bending due to wind loading are resisted solely by the 'flanges' of the module, of thickness t, the base of the tower being loaded the most, labelled as (1) in Fig. 6(b). The wind loading is again most critical when acting in the transverse direction. The imposed floor load, f, acts on each storey. The maximum normal stress in a flange at the base of the tower, which avoids yielding, can be shown to be:

$$\sigma_y \geq \sigma = \sigma_w + \frac{0.5n(n+1)hS_t}{blt}, \text{ where } \sigma_w = \frac{nw + nfbl}{2bt + 2lt} \tag{8}$$

Shear stresses are also calculated as before assuming that these are resisted by the 'webs' of the module only, area (2) in Fig. 6(b). The corresponding yield condition is:

$$\tau_y \geq \tau = \frac{nS_t}{2bt} \tag{9}$$

Two regions at the base of the tower now need to be checked: the flanges, area (1) in Fig. 6(b), under normal stresses but no shear stresses, using Eqn 8; and the webs, area (2) in Fig. 6(b), which carry normal stresses due to gravity and the imposed floor loads, σ_w, as well as shear stresses, τ, from Eqn 9. The latter combination is assessed by assuming $\sigma_y = \sqrt{3}\tau_y$ to give a yield constraint for the webs where:

$$\sigma_y \geq \sqrt{\sigma_w^2 + 3\tau^2} \tag{10}$$

A different yield criterion to that in Eqn 7 is chosen, as the shear stresses here cannot be assumed small relative to the normal stresses.

2.4.3 Unbraced frame modules

The unbraced normal and shear stresses are calculated using a similar approach to that presented above in Sections 2.4.1 & 2.4.2. The maximum normal and shear stresses experienced by the highest loaded columns of cross-sectional area A_c, area (1) in Fig. 6(c), can be calculated as:

$$\sigma_y \geq \sigma = \sigma_w \left(\frac{2bt + 2lt}{4A_c} \right) + \frac{0.5n(n+1)hS_t}{2bA_c}, \quad \tau_y \geq \tau = \frac{nS_t}{4A_c} \tag{11}$$

A linear interaction between the axial force, $F = A_c\sigma$ from Eqn 11, and the bending moment, M, in the columns is assumed for simplicity. The resulting interaction equation for the columns with the highest loading, area (1) in Fig. 6(c), is found to be:

$$\frac{F}{A_c\sigma_y} + \frac{M}{Z\sigma_y} = 1 \tag{12}$$

where $M = (nS_t/4) \times h$ and Z is the plastic section modulus.

2.4.4 Braced frame modules

For braced frames, the normal stresses are calculated as for the unbraced frames using Eqn 11, this time considering area (1) in Fig. 6(d). Due to the presence of the bracing members, there are no shear or bending stresses in the braced frames. Yielding of a brace of cross-sectional area A_{x}, is most critical when the wind acts in the transverse direction, therefore the braces labelled (3) in Fig. 6(d) are checked using:

$$\sigma_y A_{\mathrm{x}} \geq \frac{nS_t}{2}\frac{\sqrt{b^2+h^2}}{b} \tag{13}$$

2.5 Stability

After checking material failure, each relevant component is checked against buckling, which again generally occurs at the bottommost storey as this is where the columns or walls suffer the largest vertical load, as explained previously. Figure 6, which shows which module components are checked for failure, is again referred to in the following sections, where relevant.

2.5.1 Solid block modules

The bottommost solid block module cannot buckle and therefore self-weight buckling of the whole tower is considered instead using an existing theory by Greenhill (1881). This is derived from the properties of the modular towers which could contribute to self-weight buckling: the Young's modulus E; the second moment of area I; the density ρ; the width b and the length l of the module. A dimensional analysis confirms that the maximum height is proportional to $(EI/\rho gbl)^{\frac{1}{3}}$, where the constant of proportionality in Eqn 14 was obtained experimentally by Greenhill:

$$nh = 1.986\left(\frac{EI}{\rho gbl}\right)^{\frac{1}{3}} \tag{14}$$

where n is the number of storeys at the point of self-weight buckling and h is the height of one module.

2.5.2 Thin-walled box modules

The normal stresses at the bottommost storey in the thin-walled box modules are found in the flanges as discussed in Section 2.4.2. These are then converted to normal forces in each wall of the module and

compared to the critical load that would result in plate buckling, P_{crit}. An approach which assumes that the corners of the module are simple supports (Trahair et al 2008) is used to find P_{crit} of the least stable longer wall, $P_{crit,long}$, which is the wall above area (1) in Fig. 6(b):

$$P_{crit,long} = \frac{l^2}{h^2}\left(1+\frac{h^2}{l^2}\right)^2 \frac{\pi^2 E t^2}{12l^2(1-\nu^2)} \times (lt) \geq \left(\sigma_w + \frac{0.5n(n+1)hS_t}{blt}\right) \times (lt) \tag{15}$$

where ν is the Poisson's ratio and the wind loading is applied in the transverse direction, which is critical.

The shear stresses at the bottommost storey are found in the webs, the walls above (2) in Fig. 6(b), as per Section 2.4.2, but here for both the short and long walls acting as webs, depending on the direction of wind loading. They are compared to the critical shear stresses for shear plate buckling, τ_c (BSI 2006), again assuming that the web edges are simply supported for a conservative estimate:

$$\tau_{c,short} = K_{q,short}\tau_y \geq \tau_{short} = \frac{nS_t}{2bt}, \quad \tau_{c,long} = K_{q,long}\tau_y \geq \tau_{long} = \frac{nS_l}{2lt} \tag{16}$$

where S_l is the horizontal wind force per storey in the longitudinal wind direction, perpendicular to the transverse direction defined previously. The critical shear stresses for both the long, $\tau_{c,long}$, and short, $\tau_{c,short}$, walls of the bottommost module are calculated since it is unclear which wind load direction is critical. The associated reduction factors $K_{q,short}$ and $K_{q,long}$ are found (BSI 2006, Fig. 23).

The flanges, the walls above (1) in Fig. 6(b), are assumed to resist normal stresses only, using Eqn 15. However, the webs, the walls above (2) in Fig. 6(b), resist both normal stresses, σ_w, and shear stresses, Eqn 16, and these may interact. An interaction between them is assumed for the webs at failure (BSI 2006) where:

$$\frac{\sigma_w bt}{P_{crit,short}} + \left(\frac{\tau_{short}}{\tau_{c,short}}\right)^2 = 1, \quad \frac{\sigma_w lt}{P_{crit,long}} + \left(\frac{\tau_{long}}{\tau_{c,long}}\right)^2 = 1 \tag{17}$$

2.5.3 Unbraced frame modules

The forces in the highest loaded columns of the bottommost storey of the unbraced frame tower, (1) in Fig. 6(c), are compared to the elasto-plastic critical buckling load, P_{crit} (BSI 2009). P_{crit} is calculated by initially finding the plastic failure load due to yielding, $P_{pl} = A_c\sigma_y$, and the elastic failure load due to Euler buckling, assuming the column is unrestrained at the top, $P_{el} = \pi^2 EI_c/(2h)^2$, where I_c is the minor axis second moment of area of a column. After combining these, the non-dimensional slenderness $\bar{\lambda} = \sqrt{P_{pl}/P_{el}}$ can be calculated and used to obtain the appropriate reduction factor, χ (BSI 2009, Fig. 6.4). P_{pl} is then multiplied by χ to give:

$$P_{crit} = \chi P_{pl} \geq F = \sigma_w\left(\frac{2bt+2lt}{4}\right) + \frac{0.5n(n+1)hS_t}{2b} \tag{18}$$

A linear interaction between the axial force, F, and the bending moment, M, in the most critical columns, (1) in Fig. 6(c), is assumed as per Section 2.4.3:

$$\frac{F}{P_{crit}} + \frac{M}{Z\sigma_y} = 1 \tag{19}$$

Finally, the buckling failure of the beams of each module is also considered. The forces in the horizontal beams of the bottommost module, area (2) in Fig. 6(c), are the highest due to the wind loading. The forces in the beams are then compared to their Euler buckling load. Note that there are beams at the base and the top of each module, so there is a 'double-height' beam where two modules are connected, as can be seen in Fig. 6(c). Each of the two relevant double-height beams is assumed to attract an axial load equal to half of the total base shear force. Both the 'short' and 'long' beams of the modules are considered, as it is unclear which wind direction is critical:

$$P_{crit,short} = \frac{\pi^2 E I_b}{b^2} \geq \frac{nS_t}{2}, \quad P_{crit,long} = \frac{\pi^2 E I_b}{l^2} \geq \frac{nS_l}{2} \tag{20}$$

where I_b is the minor second moment of area of the double-height beam.

2.5.4 Braced frame modules

The procedure for braced frames is almost the same as that detailed in Section 2.5.3 for the columns, (1), and the beams, (2) in Fig. 6(d). The main differences are that the critical buckling load is calculated as $P_{el} = \pi^2 E I_c / h^2$, since the columns are assumed to be restrained at both ends due to the bracing; and that no moments arise, so Eqn 19 is not relevant for braced frames. Note that buckling of the bracing is not considered; cross-bracing is provided, so one brace always acts in tension.

2.6 Deflection

The SLS is considered by imposing a deflection limit (height/500) at the top storey, assuming small deflection theory. For all module topologies, the critical wind load direction is the transverse.

2.6.1 Solid block modules

Summing the wind force, S_t, over n storeys, the shear deflection is calculated as $0.5n(n+1) \times 1.5 S_t h / Gbl$, where G is the shear modulus. A further component due to flexural deflection is again obtained by summing the contribution from S_t over n storeys, and found to be $n^2(n+1)(3n+1) \times S_t h^3 / 24EI$. Adding these expressions leads to Eqn 21 for the overall maximum deflection, δ:

$$\frac{nh}{500} \geq \delta = \frac{n(n+1)}{2} \frac{3}{2} \frac{S_t h}{Gbl} + \frac{S_t h^3}{24EI} n^2 (n+1)(3n+1) \tag{21}$$

where I is the second moment of area of a solid block about its minor axis.

2.6.2 Thin-walled box modules

A similar approach to that used in Section 2.6.1 is undertaken leading to:

$$\frac{nh}{500} \geq \delta = \frac{n(n+1)}{2}\frac{3}{4}\frac{S_t h}{Gbt} + \frac{S_t h^3}{24EI}n^2(n+1)(3n+1) \tag{22}$$

where I is the minor second moment of area of the thin-walled module.

2.6.3 Unbraced frame modules

The deflection at the top storey is calculated somewhat differently for the unbraced frames. Each frame is assumed to have a full moment connection at the top of each column, and a pinned connection at the base. The deflection of each frame is firstly found separately per storey as $0.5S_t \times (h^3/6EI_c + bh^2/12EI_b)$, where I_c and I_b are the second moments of area of the column and beam, respectively. Summing over n storeys, the overall deflection at the top is found to be:

$$\frac{nh}{500} \geq \delta = \frac{n(n+1)}{2}\frac{S_t}{2}\left(\frac{h^3}{6EI_c} + \frac{bh^2}{12EI_b}\right) \tag{23}$$

2.6.4 Braced frame modules

For the braced frame modules, a displacement diagram is drawn for a one and a two storey tower and the results are extrapolated by summing each deflection component from the displacement diagrams over n storeys, as shown in Eqn 24. The first component, $(S_t(h^2+b^2)\cos\theta/2bEA_{\mathrm{x}}) \times (n(n+1)/2)$, arises from superposing the extensions of the cross-braces in the displacement diagrams, each lying at an angle θ to the horizontal; the second component, $(S_t h(h^2+b^2)\sin\theta/2b^2EA_{\mathrm{x}}) \times (n(n+1)/2)$, is associated with the rotations of the cross-braces; the third component, $(S_t h^3/2b^2EA_c) \times (n(n+1)(3n^2+n+2)/12)$, is connected with the deflections of the columns; and the fourth component, $(S_t b/4EA_b) \times (n(n+1)/2)$, arises due to the deflections of the beams. The final expression is:

$$\begin{aligned}\frac{nh}{500} \geq \delta = {} & \frac{S_t(h^2+b^2)\cos\theta}{2bEA_{\mathrm{x}}}\left(\frac{n(n+1)}{2}\right) + \frac{S_t h(h^2+b^2)\sin\theta}{2b^2EA_{\mathrm{x}}}\left(\frac{n(n+1)}{2}\right) \\ & + \frac{S_t h^3}{2b^2EA_c}\left(\frac{n(n+1)(3n^2+n+2)}{12}\right) + \frac{S_t b}{4EA_b}\left(\frac{n(n+1)}{2}\right)\end{aligned} \tag{24}$$

2.7 Ashby-inspired Charts

The constraint equations in the previous sections for each module topology are solved to obtain the critical height of tower for each failure mode, for numerous design variables, such as module size and structural section size. Here, the pair of metrics on each chart are the critical height of modular tower against the self-weight per module, and the charts include boundaries enclosing data from the different module topologies in order to describe their combined behaviour. Each point on the charts represents a modular tower, found by calculating the height at which any part of the tower exceeds ULS or SLS. The charts are presented as log-log plots in keeping with the spirit of the original Ashby Charts and also because this shows the data most clearly. A Microsoft Excel spreadsheet is used to solve the equations in Sections 2.4 – 2.6 for the critical heights. A finite element (FE) analysis is used to verify some of the results using Oasys GSA (Arup 2015).

The module dimensions are selected according to the extreme heights, widths and lengths in Table 1, following existing module dimension ranges in the literature. The size of the modules can be any combination of the range of these dimensions resulting in many possible module sizes. However, to reduce the number of permutations, just eight module sizes are extracted, combining in turn each of the smallest and largest dimensions in Table 1. It is reasonable to assume that by considering the extreme values, these data points would enclose all other combinations on the chart, thereby defining the desired cluster boundaries.

	Height, h [m]	**Width, b [m]**	**Length, l [m]**
Smallest	2.5	2.5	5
Largest	4	4	12

TABLE 1: Smallest and largest module dimensions (Lawson 2007)

For thin-walled box modules, three different wall types are considered: walls made from flat sheets of steel; walls made from cold formed sections; and walls made from corrugated steel sheets. The behaviour for the latter two is simplified by calculating two equivalent flat sheet thicknesses of the walls: a wall thickness that gives the same cross-sectional area for calculating weight and strength, and a second wall thickness that leads to the same stiffness for calculating buckling and deflection. The sections used and their properties are shown in the Appendix, which are at the extremes of very thin and very thick walls, and are then considered with each of the eight previous overall module sizes, in order to obtain the relevant cluster boundaries.

Commercially available steel sections are considered for the braced and unbraced frames because the section properties are readily available. Both hot rolled and cold formed steel sections are used. Beam cross-sections considered include universal beams, rectangular hollow sections and channel sections, and column cross-sections include universal columns, circular hollow sections and square hollow sections. The largest and smallest sections of each beam cross-section are paired with the largest and smallest sections of each column

cross-section in turn, in order to obtain a boundary for all steel sections on the charts. Therefore, many module combinations and hence many different modular towers made from frame modules are expected. The analysis is extended to include the mean, upper and lower quartile sizes of the steel sections, in order to verify the cluster boundaries found. For the braced frames, mild steel flat sections are used for the bracing. The steel sections considered for the frames and their properties are given in the Appendix.

3 Results and discussion

3.1 The module topology Ashby-inspired Chart

Figure 7 shows the charts for the critical limit of either material failure, stability or deflection, with the colours representing different module topologies. Note that although module sub-types, *e.g.* hot rolled and cold formed steel sections for the frame modules, are indicated on the chart, only overall module topologies are highlighted using balloon boundaries for clarity.

Figure 7(a) shows the critical limit of either ULS or SLS for each module combination. This chart is needed for a complete design when buildings comply with both the ULS and the SLS requirements, and can be used in two ways. First, for a given self-weight of a module, the maximum possible height can be found; second, for a required height, the lightest modular tower possible can be found by choosing the combination furthest to the left, either in absolute terms or for a certain module topology. The chart also indicates the height at which it is necessary to use an external framed modular construction, *i.e.* when the desired height is not possible using the stacked module construction assumed here.

Figure 7(a) shows that, as we might expect, generally the maximum heights possible are achieved using solid block modules, which represents an upper, albeit unpractical, limit. For a more realistic module topology, unbraced frames seem to outperform the other two module topologies, which is rather surprising, and the maximum of which is 78 storeys. However, since this chart represents an initial, conceptual design, it is thought that this is partially due to the initial assumptions made. In particular, the moment connections in the unbraced frame are taken as rigid; in reality however, they will be flexible, resulting in a larger unbraced frame deflection and, hence, a smaller maximum height. Also, choosing a larger brace section in the braced frames would result in a smaller deflection, giving a larger maximum height. Only two different brace cross-section sizes were tried in this analysis due to time constraints.

Considering the cluster boundaries, all the module topologies, except the solid blocks, provide a large range of heights, with the unbraced frame cluster providing taller towers than thin-walled boxes or braced frames. Furthermore, solid blocks are the heaviest, thin-walled boxes are generally the lightest, unbraced frames have a narrow range of self-weights, and braced frames have a wide range of self-weights. Light thin-walled boxes are a favourable design because it is advantageous for modules to be light for construction

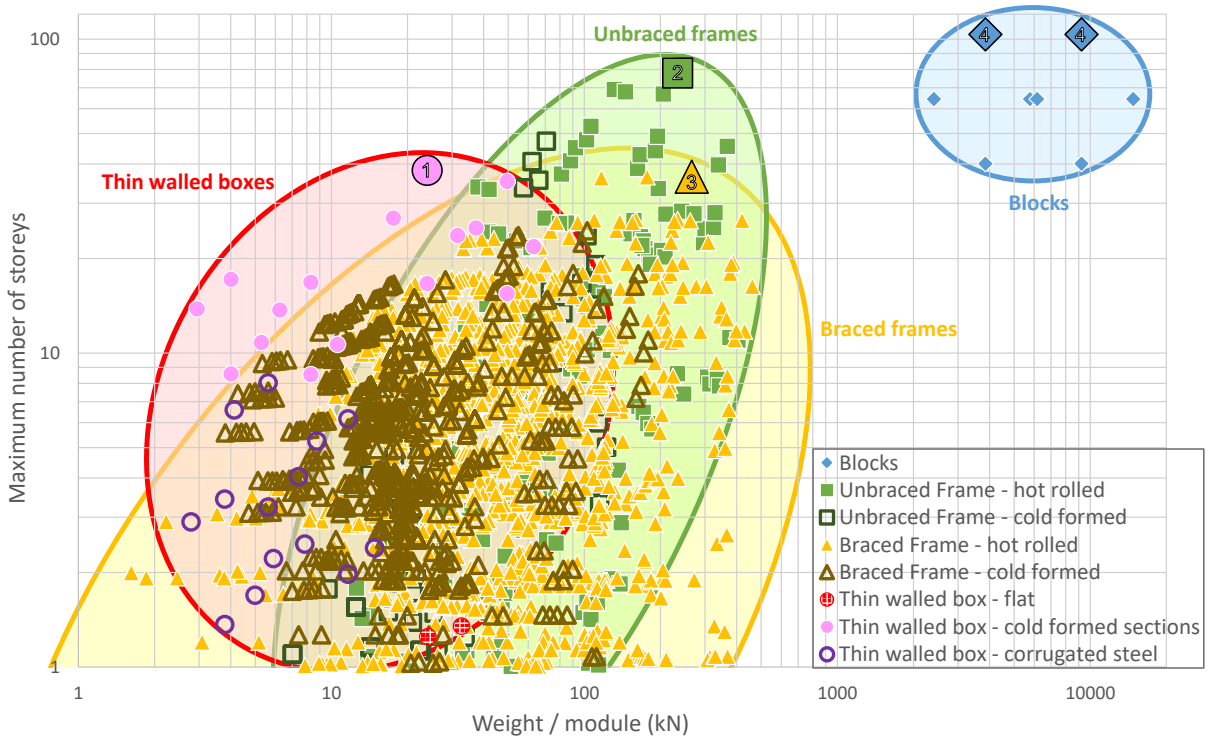

(a)

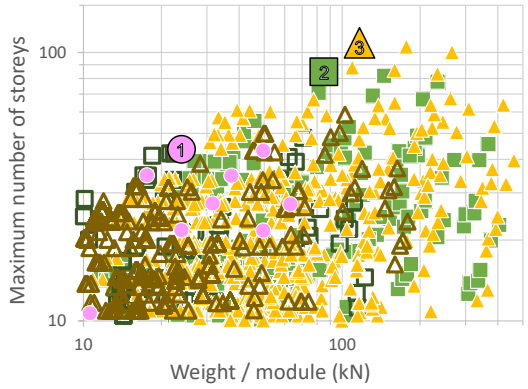

(b)

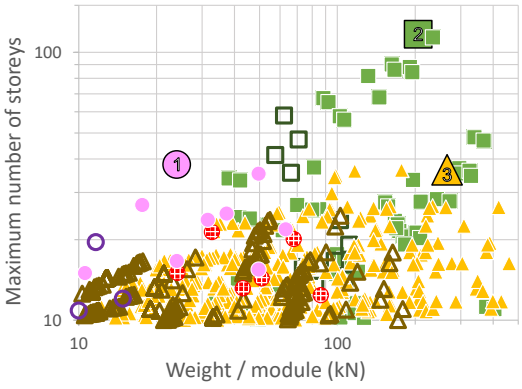

(c)

FIGURE 7: The module topology Ashby-inspired Chart, showing the self-weight per module against maximum height. Note that the legend is valid for all three charts. **(a)** Overall Ashby-inspired Chart, considering the most critical of either ULS or SLS. Each data point represents a different modular tower and balloons are used to cluster results together: circles, thin-walled boxes; squares, unbraced frames; triangles, braced frames; diamonds, solid blocks. The tallest modular tower for each module topology is highlighted: (1) thin-walled boxes; (2) unbraced frames; (3) braced frames; (4) solid blocks. **(b)** ULS Chart, as (a), but considering only ULS. This chart is magnified to better show the relevant results. **(c)** As (b), but for SLS

purposes. For module sub-types, it is observed that hot rolled sections generally provide taller modular towers than cold formed sections for the frame modules. Thin-walled boxes constructed from cold formed sections result in taller towers than if made from flat or corrugated steel sheet walls. This demonstrates that if the data is plotted in this way, a lot of design information can be obtained from the general properties of the cluster boundaries alone.

By considering ULS and SLS requirements separately, it is possible to show the critical limit state for each module topology in Figs 7(b) & (c). The ULS data is plotted in Fig. 7(b). Here, the best performing module is a braced frame, showing that it is the SLS which lowers the maximum height of the braced frames, and hence the unbraced frames performing better overall for the current assumptions. Figure 7(c) shows the SLS performance, where, like the overall chart in Fig. 7(a), it is the unbraced frames greatly outperforming the others. More generally, there are many more solutions on the ULS plot, which implies that higher towers may be achieved if the SLS deflections can be reduced, since currently for most modules SLS is critical.

3.2 The failure mechanism Ashby-inspired Chart

Figure 8 displays the same data as Fig. 7(a) except now we indicate the failure mechanisms instead of the module topologies. The two dominant failure mechanisms for the tallest towers are stiffness dominated: buckling of the columns and lateral deflection, as we might expect for tall lightweight buildings. Boundaries have not been drawn here, because these would generally overlap with each other, except for the strength of columns/walls mechanism and deflection of the solid blocks (top right corner). The buckling of columns/walls and deflection mechanisms would essentially form the same boundary, and the buckling of beam boundary would be similar, but with lower maximum heights. Ultimately, the chart reveals that taller modular buildings typically fail due to a lack of stiffness.

3.3 The robustness analysis Ashby-inspired Charts

The use of unbraced frames results in taller modular towers than braced frames. This seems unrealistic as we might expect the braced frame to be stiffer, thereby increasing the maximum possible height. Therefore, a robustness analysis is carried out on the material properties used, namely, the Young's modulus (and shear modulus) and the yield strength, with Fig. 9 displaying the relevant charts obtained. Here, the comparison is between the data points using a different Young's modulus or yield strength and the original data. To test the robustness of the charts, these parameters are changed to firstly be reduced and then increased from their original values, to ensure that the form of the charts is not due to the chosen values of Young's modulus or yield strength. Figure 9(a) shows the results for a Young's modulus reduced tenfold from its original value of 210 GPa. It can be observed that the maximum heights of the data points are generally

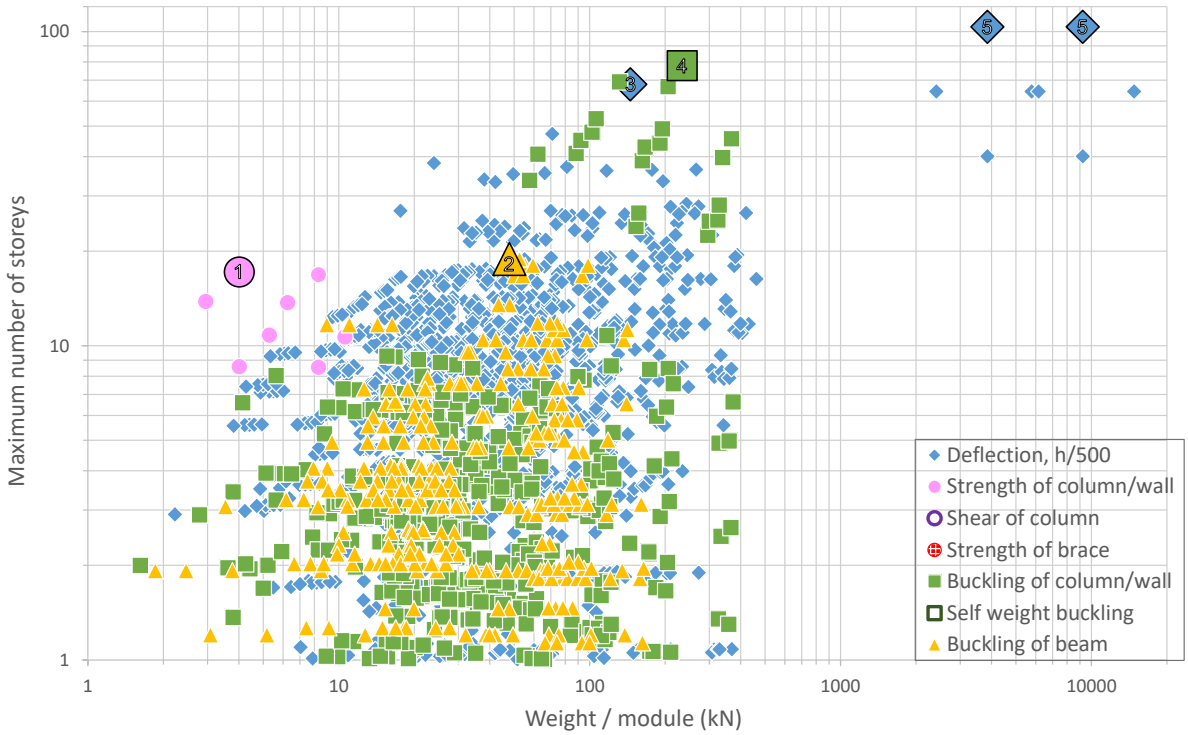

FIGURE 8: The failure mechanism Ashby-inspired Chart, showing the same results as Fig. 7(a), with the data point shapes here representing the limiting failure mechanism of each modular tower. The tallest modular towers for each failure mechanism are highlighted: (1) material (strength) failure of a column/wall in the module; (2) buckling of a beam in a frame module; (3) "failure" in deflection (exceeding height/500) for realistic modules only, *i.e.* excluding solid blocks; (4) buckling of a column/wall; (5) "failure" in deflection for blocks

reduced, with the height of the tallest modular tower reduced by about fivefold. The module topology and failure mechanism of the tallest modular tower changes from an unbraced frame to a thin-walled box and from a column buckling to a deflection 'failure' respectively. These changes in response are due to the highly non-linear failure mechanism behaviour, where changes in modulus are not met by proportional changes in ultimate heights. This is demonstrated further in Fig. 9(b), which shows the results when the Young's modulus is increased by about five times its original value, giving an overall increase in maximum height of all data points; the tallest tower is now approximately 20% taller, and its module topology and failure mechanism are the same as the original results. Furthermore, more points become visible on the chart, reinforcing the observation that the dominant failure mechanisms in the original results are stiffness related.

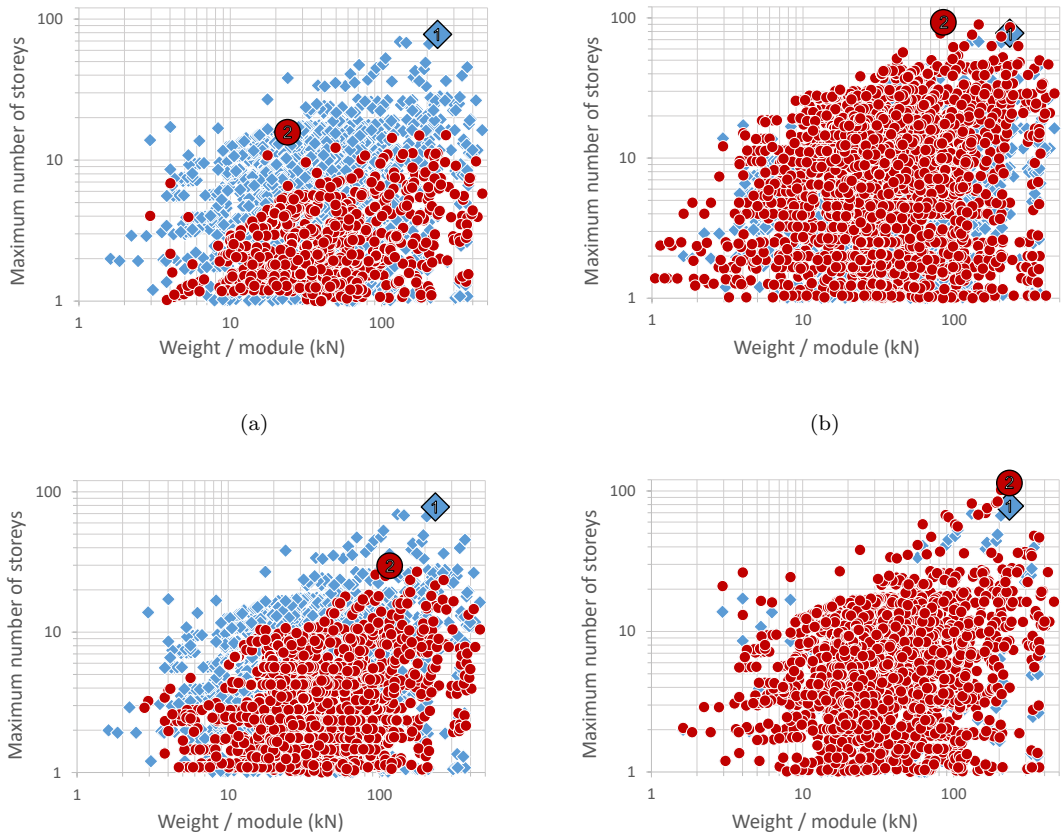

FIGURE 9: The robustness analysis Ashby-inspired Charts, with varying material properties. Original material property results are diamonds (same data as Figs 7(a) & 8, but here all data points are represented by the same shape) and new material property results are circles: **(a)** Young's modulus reduced to 21 GPa. (1) Original maximum height 78 storeys, unbraced frame module, column buckling failure mechanism, (2) new maximum height 16 storeys, thin-walled box module, deflection "failure" mechanism; **(b)** Young's modulus increased to 1000 GPa. (1) as (a), (2) 93 storeys, unbraced frame, column buckling; **(c)** yield strength reduced to 35.5 MPa: (1) as (a), (2) 30 storeys, braced frame, column material (strength) failure; **(d)** yield strength increased to 1000 MPa: (1) as (a), (2) 114 storeys, unbraced frame, deflection "failure"

Figure 9(c) shows the results when the yield strength is reduced by ten times its original value of 355 MPa. The tallest tower height is now approximately 2.5 times smaller than the original maximum, with the module topology and failure mechanism altering from an unbraced to a braced frame and from column buckling to a material failure, respectively. When instead the yield strength is increased approximately threefold, much of the data remains the same as the original results, however the maximum height increases by about 50%. The unbraced frame module giving maximum height does not change from the original results but it now 'fails' by deflection instead of column buckling. Hence, increasing the yield strength enables the height

to increase until another failure mode is incurred. The fact that the yield strength data does not change significantly from the original results further reinforces the conclusion that the strength is generally not a limiting design factor.

Based on this limited robustness analysis, it can be concluded that the superior performance of the unbraced frames is not due to the chosen material properties: increasing their values achieves taller towers, as expected, but the unbraced frames still provide the tallest towers. Reducing their values is not conclusive, since the module topology providing the tallest towers changes from the original results, which suggests that further work needs to be undertaken. Figure 9 also shows that altering a material property by a factor does not change the maximum number of storeys by the same factor; as noted, this non-linearity arises due to the interactions between the many different failure mechanisms considered. If boundaries were to be drawn around the collective data points of different module topologies, as in the original chart (Fig. 7(a)), they would shift up or down, but they would also change shape due to this non-linearity.

3.4 Limitations

The charts presented here intend to show the height limits which can be reached as well as the module topologies which provide the lightest structures, but only as an initial conceptual design, since they do not currently consider practicalities. Future improvements may include: incorporating a practical upper (or lower) limit of section size as a constraint; limiting the allowable module weight to facilitate installation; and including the extra stiffness contribution from non-structural elements, such as infill walls. It should also be noted that, since unfactored loads have been used throughout, the design maximum heights will in practice be lower than the heights calculated here.

4 Conclusions

Ashby Charts have been previously used for many design applications, most prominently in material design and later followed by structural section design. Here, they have further been expanded to the design of an overall structure, namely the design of a stacked modular tower. It was found that a pure Ashby design approach would result in a chart with too many variables and hence axes. Therefore, three different module topologies (thin-walled boxes, unbraced frames and braced frames) were investigated, considering ULS and SLS requirements, using a traditional design approach. The metrics plotted on the Ashby-inspired Charts were maximum height against weight of a single module.

'The module topology Ashby-inspired Chart' has been developed as a design tool for choosing the desired module topology which meets certain requirements such as a prescribed tower height or weight of a module. It is also found that the tallest tower is achieved using unbraced frame modules, hence the chart suggesting

that this module topology is preferential for a very tall modular building. But this limit should be treated with caution, since only initial concept design considerations have been taken into account and factors such as practical section sizes, the need to provide full-moment connections, the influence of non-structural components and the use of unfactored loads have not. However, these could be considered at a later design stage and the chart can be updated. 'The failure mechanism Ashby-inspired Chart' shows that, for most module topologies, stiffness failure modes such as excessive deflections and buckling are critical for taller modular towers. If the required deflection limits can be relaxed or the material or structure stiffened, even taller buildings may be achieved.

An unintuitive outcome is that unbraced frames outperform braced frames. A material property robustness analysis has been performed and the corresponding charts show that unbraced frames still achieve the maximum tower height when the Young's modulus and yield strength of the steel are increased. However, other module topologies outperform the unbraced frames when those material properties are reduced. Further investigation is needed, but the result that unbraced frames achieve the tallest modular towers is still valid for the assumptions made.

Finally, the Ashby-inspired Charts hold promise for structural engineering applications beyond the modular buildings considered here. Modular towers were chosen as a simple initial study to demonstrate that Ashby-inspired Charts can be used at an overall structure level, as well as for structural sections or materials.

Acknowledgements

We are grateful to Professor Mike Ashby for his helpful comments and feedback on a draft of this manuscript. We also thank Simon Smith of Smith and Wallwork Engineers for his involvement. This study was funded by the Engineering and Physical Sciences Research Council Centre for Doctoral Training in Future Infrastructure and Built Environment (grant reference: EP/L016095/1).

Appendix: Steel section sizes

The steel section sizes used in the analysis are listed below in Tables 2, 3 and 4 (Tata Steel 2016a,b; Kingspan Group 2010; Cobb 2004):

Flat	Thickness (weight) [mm]	Thickness (stiffness) [mm]	I [cm^4/m]
Minimum	0.5	0.5	1.04×10^{-3}
Maximum	5	5	1.04

Corrugated	Section	Thickness (weight) [mm]	Thickness (stiffness) [mm]	I [cm^4/m]
Minimum	Tata Trisobuild Wall Profile C19	0.58	7.3	3.24
Maximum	Tata Trisobuild Wall Profile C32	0.86	11.6	13.0

Cold formed sections	Section	Area [cm^2]	I_{maj} [cm^4]	Spacing [mm]	Thickness (weight) [mm]	Thickness (stiffness) [mm]	I [cm^4/m]
Minimum	Kingspan Multichannel L145070120	3.68	125.52	600	0.613	29.3	210
Maximum	Kingspan Multichannel L350090270	14.63	2526.07	400	3.66	91.2	6321

TABLE 2: Thin-walled boxes section sizes for flat sheet wall boxes, corrugated sheet wall boxes and boxes with walls made from cold formed sections

UKB	Section	Area [cm^2]	I_{maj} [cm^4]	I_{min} [cm^4]
Minimum	127 × 76 × 13	16.5	473	55.7
Lower quartile	305 × 127 × 48	61.2	9570	461
Mean	686 × 254 × 125	159	118000	4380
Upper quartile	686 × 254 × 170	217	170000	6630
Maximum	1016 × 305 × 487	620	1020000	26700

PFC	Section	Area [cm^2]	I_{maj} [cm^4]	I_{min} [cm^4]
Minimum	100 × 50 × 10	13	208	32.3
Lower quartile	200 × 75 × 23	29.9	1960	170
Mean	200 × 90 × 30	37.9	2520	314
Upper quartile	260 × 90 × 35	44.4	4730	353
Maximum	430 × 100 × 64	82.1	21900	722

RHS	Section	Area [cm^2]	I_{maj} [cm^4]	I_{min} [cm^4]
Minimum	50 × 30 3	4.34	13.6	5.94
Lower quartile	120 × 60 8	25.6	425	135
Mean	200 × 100 12.5	67.1	3140	1000
Upper quartile	300 × 250 8.8	92.9	12400	9390
Maximum	500 × 300 20	300	98800	44100

UKC	Section	Area [cm^2]	I_{maj} [cm^4]	I_{min} [cm^4]
Minimum	152 × 152 × 23	29.2	1250	400
Lower quartile	254 × 254 × 73	93.1	11400	3910
Mean	356 × 368 × 177	226	57100	20500
Upper quartile	356 × 368 × 202	257	66300	23700
Maximum	356 × 406 × 634	808	275000	98100

EQA	Section	Area [cm^2]	I_{maj} [cm^4]	I_{min} [cm^4]
Minimum	90 × 90 7	12.2	147	38.3
Lower quartile	100 × 100 10	19.2	280	73
Mean	150 × 150 12	34.8	1170	303
Upper quartile	150 × 150 15	43	1430	370
Maximum	200 × 200 24	90.6	5280	1380

CHS	Section	Area [cm^2]	I [cm^4]
Minimum	21.3 2.6	1.53	0.681
Lower quartile	48.3 6.3	8.31	18.7
Mean	168.3 10	49.7	1560
Upper quartile	244.5 10	73.7	5070
Maximum	508 16	247	74900

SHS	Section	Area [cm^2]	I [cm^4]
Minimum	40 × 40 3	4.34	9.78
Lower quartile	70 × 70 7.1	17.3	112
Mean	160 × 160 10	58.9	2190
Upper quartile	180 × 180 12.5	82.1	3790
Maximum	400 × 400 20	300	71500

Mild steel flat	Area [cm^2]
Minimum	1
Lower quartile	5.8
Mean	16.8
Upper quartile	22.5
Maximum	100

TABLE 3: Hot rolled frames section sizes; beam sections are UKB, PFC, and RHS; column sections are UKC, EQA, CHS and SHS; bracing sections are mild steel flats

Kingspan Eaves Beam	Section	Area [cm^2]	I_{maj} [cm^4]	I_{min} [cm^4]
Minimum	E185140	6.39	356.59	58.32
Lower quartile	E215170	7.24	512.28	66.04
Mean	E265150	8.08	835.55	72.5
Upper quartile	E265150	8.08	835.55	72.5
Maximum	E265200	11.53	1191.52	103.39

Kingspan Multichannel	Section	Area [cm^2]	I_{maj} [cm^4]	I_{min} [cm^4]
Minimum	L145070120	3.68	125.52	26.07
Lower quartile	L205070150	5.48	348.43	36.04
Mean	L300090150	7.42	989.64	74.1
Upper quartile	L300090180	8.91	1184.14	87.76
Maximum	L350090270	14.63	2526.07	130.99

RHS	Section	Area [cm^2]	I_{maj} [cm^4]	I_{min} [cm^4]
Minimum	50 × 25 2	2.74	8.38	2.81
Lower quartile	100 × 60 3.5	10.4	137	61.9
Mean	250 × 150 5	38.4	3300	1510
Upper quartile	180 × 100 10	48.6	1860	736
Maximum	500 × 300 12.5	187	62700	28700

CHS	Section	Area [cm^2]	I [cm^4]
Minimum	33.7 3	2.89	3.44
Lower quartile	168.3 5	25.7	856
Mean	355.6 6.3	69.1	10500
Upper quartile	508 6.3	99.3	31200
Maximum	508 16	247	74900

SHS	Section	Area [cm^2]	I [cm^4]
Minimum	25 × 25 2	1.74	1.48
Lower quartile	90 × 90 3.5	11.8	145
Mean	200 × 200 6.3	47.4	2920
Upper quartile	200 × 200 10	72.6	4250
Maximum	400 × 400 12.5	187	45900

TABLE 4: Cold formed frames section sizes; beam sections are Kingspan Eaves Beam, Kingspan Multichannel and RHS; column sections are CHS and SHS; bracing sections are mild steel flats (as Table 3)

References

American Society of Civil Engineers: Task Committee on Drift Control of Steel Building Structures of the Committee on Design of Steel Building Structures (1988) 'Wind Drift Design of Steel-framed Buildings: State-of-the-art Report.' *ASCE Journal of Structural Engineering* 114(9): 2085-2108. DOI: 10.1061/(ASCE)0733-9445(1988)114:9(2085).

Ashby MF (1972) 'A first report on deformation-mechanism maps.' *Acta Metallurgica* 20(7): 887–897. DOI: 10.1016/0001-6160(72)90082-X

Ashby MF (1989) 'Overview no. 80: On the engineering properties of materials.' *Acta Metallurgica* 37(5): 1273–1293. DOI: 10.1016/0001-6160(89)90158-2

Ashby MF (2005) *Materials selection in mechanical design.* Butterworth-Heinemann, Boston

Ashby MF and Brechet YJM (2003) 'Designing hybrid materials.' *Acta Metallurgica* 51(19): 5801–5821. DOI: 10.1016/S1359-6454(03)00441-5.

Ashby MF, Gandhi C and Taplin DMR (1979) 'Overview no. 3: Fracture-mechanism maps and their construction for F.C.C. metals and alloys.' *Acta Metallurgica* 27(5): 699–729. DOI: 10.1016/0001-6160(79)90105-6

Ashby MF and Greer AL (2006) 'Metallic glasses as structural materials.' *Scripta Materialia* 54(3): 321–326. DOI: 10.1016/j.scriptamat.2005.09.051

Arup (2015) *Oasys GSA* (Version 8). Computer program. URL: `www.oasys-software.com`.

Begley MR, Philips NR, Compton BG, Wilbrink DV, Ritchie RO, and Utz M (2012) 'Micromechanical models to guide the development of synthetic 'brick and mortar' composites.' *Journal of the Mechanics and Physics of Solids* 60(8): 1545–1560. DOI: 10.1016/j.jmps.2012.03.002

Birmingham RW, Chandler HW, Wilcox JAD and Marshall AL (1994) 'Graphical model for compression struts that integrates material and form in structural design.' *Journal of Engineering Design* 5(3): 227–240. DOI: 10.1080/09544829408907885

Birmingham RW and Wilcox JAD (1993) 'Charting the links between material selection and elemental form in structural design.' *Journal of Engineering Design* 4(2): 127–140. DOI: 10.1080/09544829308914777

British Standards Institution (2005) *UK National Annex to Eurocode 1: Actions on structures – Part 1-1: General actions – Densities, self-weight, imposed loads for buildings.* British Standards Institution, London

British Standards Institution (2006) *BS 5400-3:2000: Steel, concrete and composite bridges – Part 3: Code of practice for design of steel bridges*. British Standards Institution, London

British Standards Institution (2009) *BS EN 1993-1-1:2005 Eurocode 3: Design of steel structures. General rules and rules for buildings*. British Standards Institution, London

Calladine CR (1985) *Plasticity for Engineers*. Ellis Horwood, Chichester

Cobb F (2004) *Structural engineer's pocket book*. Second edition. Elsevier Butterworth-Heinemann, London

Counts WA, Frik M, Raabe D and Neugebauer J (2009) 'Using ab initio calculations in designing bcc mgli alloys for ultra-lightweight applications.' *Acta Materialia* 57(1): 69–76. DOI: 10.1016/j.actamat.2008.08.037

Counts WA, Frik M, Raabe D and Neugebauer J (2010) 'Ab initio guided design of bcc ternary mglix (x=ca, al, si, zn, cu) alloys for ultra-lightweight applications.' *Advanced Engineering Materials* 12(7): 572–576. DOI: 10.1002/adem.200900308

Crossman FW and Ashby MF (1975) 'The non-uniform flow of polycrystals by grain-boundary sliding accommodated by power-law creep.' *Acta Metallurgica* 23(4): 425–440. DOI: 10.1016/0001-6160(75)90082-6

Edkins K (2014) *Victoria Hall, 2014*. Photograph. URL: `www.geograph.ie/photo/3954915` (accessed 11/12/17)

Gandhi C and Ashby MF (1979) 'Overview no. 5: Fracture-mechanism maps for materials which cleave: F.C.C., B.C.C. and H.C.P. metals and ceramics.' *Acta Metallurgica* 27(10): 1565–1602. DOI: 10.1016/0001-6160(79)90042-7

Gorgolewski M, Grubb PJ and Lawson RM (2001) *P272: Modular construction using light steel framing*. Steel Construction Institute, Ascot: URL: `www.steelconstruction.info/File:SCI_P272.pdf` (accessed 08/12/16)

Greenhill AG (1881) 'Determination of the greatest height consistent with stability that a vertical pole or mast can be made, and the greatest height to which a tree of given proportions can grow.' *Proceedings of the Cambridge Philosophical Society* 4: 65-73

Holloway L (1998) 'Materials selection for optimal environmental impact in mechanical design.' *Materials & Design* 19(4): 133–143. DOI: 10.1016/S0261-3069(98)00031-4

Kingspan Group (2010) *Kingspan Multibeam Technical Handbook*. URL: `www.kingspanpanels.co.uk/structural/products/purlin-sheeting-rails/multibeam/` (accessed 13/12/16).

Kingspan Steel Building Solutions (image reproduced with permission) (2007) *P348: Building Design Using Modules, Figure 11*. Photograph. URL: www.steelconstruction.info/File:SCI_P348.pdf (accessed 11/12/17)

Kingspan Steel Building Solutions (image reproduced with permission) (2012) *N2 Fig7*. Photograph. URL: www.steelconstruction.info/File:N2_Fig7.png (accessed 11/12/17)

Lawson RM (2007) *P348: Building Design Using Modules*. Steel Construction Institute, Ascot. URL: www.steelconstruction.info/File:SCI_P348.pdf (accessed 08/12/16)

Lim SC and Ashby MF (1987) 'Overview no. 55 wear-mechanism maps.' *Acta Metallurgica* 35(1): 1–24. DOI: 10.1016/0001-6160(87)90209-4

Liu Y, Asthana R, and Rohatgi P (1991) 'A map for wear mechanisms in aluminium alloys.' *Journal of Materials Science* 26(1): 99–102. DOI: 10.1007/BF00576038

Malakondaiah G, and Rama Rao P (1981) 'Creep of alpha-titanium at low stresses.' *Acta Metallurgica* 29(7): 1263–1275. DOI: 10.1016/0001-6160(81)90017-1

Malakondaiah G, and Rama Rao P (1982) 'Viscous creep of β-co.' *Materials Science and Engineering* 52(3): 207–221. DOI: 10.1016/0025-5416(82)90148-3

Nemat-Nasser S, Willis JR, Srivastava A, and Amirkhizi AV (2011) 'Homogenization of periodic elastic composites and locally resonant sonic materials.' *Physical Review B* 83(10): 104103. DOI: 10.1103/PhysRevB.83.104103

Sandeman KG (2012) 'Magnetocaloric materials: The search for new systems.' *Scripta Materialia* 67(6): 566–571. DOI: 10.1016/j.scriptamat.2012.02.045

Shah DU (2013) 'Developing plant fibre composites for structural applications by optimising composite parameters: A critical review.' *Journal of Materials Science* 48(18): 6083–6107. DOI: 10.1007/s10853-013-7458-7

Shanley FR (1960) *Weight-strength analysis of aircraft structures*. Second edition. Dover Publications, New York

Sobczak L, Lang RW, and Haider A (2012) 'Polypropylene composites with natural fibers and wood general mechanical property profiles.' *Composites Science and Technology* 72(5): 550–557. DOI: 10.1016/j.compscitech.2011.12.013

Tata Steel (2016a) *The Tata Steel sections interactive 'Blue Book'*. URL: tsbluebook.steel-sci.org/EN/Browsers/Main.htm (accessed 13/12/16)

Tata Steel (2016b) *Trisobuild Wall Profiles*. URL: www.tatasteelconstruction.com/en_GB/Products/Building-envelope/Walls/Built-up-and-single-skin-systems/Sinusoidal-profiles/ (accessed 13/12/16)

Trahair NS, Bradford MA, Nethercot DA and Gardner L (2008) *The Behaviour and Design of Steel Structures to EC3*. Fourth edition. Taylor & Francis, Abingdon

Weaver PM and Ashby MF (1996) 'The optimal selection of material and section-shape.' *Journal of Engineering Design* 7(2): 129–150. DOI: 10.1080/09544829608907932

Weaver PM and Ashby MF (1998) 'Material limits for shape efficiency.' *Progress in Materials Science* 41(12): 61–128. DOI: 10.1016/S0079-6425(97)10034-2

Wegst UGK and Ashby MF (2004) 'The mechanical efficiency of natural materials.' *Philosophical Magazine* 84(21): 2167–2186. DOI: 10.1080/14786430410001680935